ACS APPLIED MATERIALS & INTERFACES

Letter

www.acsami.org

Facile Synthesis of Superparamagnetic Fe_3O_4@polyphosphazene@Au Shells for Magnetic Resonance Imaging and Photothermal Therapy

Ying Hu,[†] Lingjie Meng,*[,†,‡] Lvye Niu,[†] and Qinghua Lu*[,†,§]

[†]School of Chemistry and Chemical Technology and [§]State Key Laboratory of Metal Matrix Composites, Shanghai Jiao Tong University, Shanghai, 200240, P. R. China

[‡]School of Science, Xi'an Jiao Tong University, Xi'an, 710049, P. R. China

Supporting Information

ABSTRACT: Multifunctional nanoparticles were prepared by directly welding superparamagnetic Fe_3O_4 nanoparticles and Au shells together with highly cross-linked polyphosphazene as "glue" in a facile but effective way. The as-prepared particles can simultaneously take advantages of both magnetization of Fe_3O_4 core for magnetic resonance imaging diagnosis and strong near-infrared absorption of Au nanoshell for photothermal therapy.

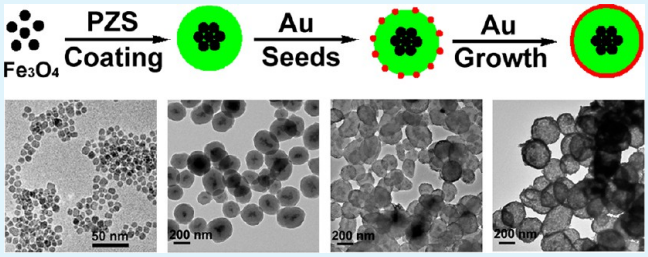

KEYWORDS: *superparamagnetic, Fe_3O_4 nanoparticles, polyphosphazene, Au nanoshells*

1. INTRODUCTION

Because of their unique optical, electrical, magnetic, and enhanced permeability and retention (EPR) properties and their sizes comparable to that of biomolecules, nanostructured materials have attracted a lot of interest for the use as drug carriers and as bioimaging, diagnostic, and therapeutic agents in biomedical applications.[1−4] Recently, multifunctional nanoparticles that incorporate both therapeutic agents and diagnostic imaging agents have been emerging as the next-generation platform in the field of nanomedicine.[3,5] Their capability to simultaneously diagnose, treat, and evaluate the efficacy may provide them the advantage over imaging agents and conventional chemotherapies to improve the quality of the patient's life.

Magnetic resonance imaging (MRI) is a powerful and noninvasive technique for medical imaging of cancers and other tissues. Superparamagnetic iron oxide nanoparticles (SIOP) are gaining popularity as a MRI contrast agent for early cancer diagnosis, because of their high relaxivity, excellent contrast effect, and low cost.[6,7] Meanwhile, the near-infrared (NIR) photothermal ablation technologies are also intriguing because they have the lowest absorption of blood and tissues in the NIR region and their implementation is noninvasive and relatively sample.[8−10] The procedure localizes optical absorbing agents at a cancer site, and then irradiates the site with a laser to "bake" the cancer cells. Au nanoparticles, including nanorods,[11,12] nanoshells,[13,14] and nanocages,[15−17] are often used as absorbing agents for their nature of strong surface Plasmon resonance (SPR) at NIR region. Several successful examples have been illustrated with Au shell-coated SIOP using silicon oxide, carbon and block polymers as "glues".[18−21] The combination of magnetization and SPR, a so-called magnetoplasmonic assembly, provides the complement of both properties in terms of cancer diagnosis, detection of biological processes, and therapy.

The design and preparation of the "glue" layer is an important issue for achieving the multifunctional particles. An ideal glue layer should be well-coated on SIOP to endow them with physical and chemical stability. It should also have a lot of metal binding groups which are ready to attach gold ions/atoms to facilitate the growth of gold nanoshells. In addition, it is expected to have a good biocompatibility and thermal stability. Poly(cyclotriphosphazene-co-4,4′-sulfonyldiphenol) (PZS) is a versatile, highly cross-linked polymer with outstanding thermal stability, solvent resistance, water dispersibility and biocompatibility, and has been successfully used to coat different nanomaterials.[22,23] It is rich in N, P, and S atoms and has plenty of phenolic hydroxyl groups to interact with a noble metal.[24] Therefore, PZS appears to meet all the relevant criteria to be the ideal "glue" layer for Au shell-coated SIOP. Herein, we demonstrated a facile but effective approach to synthesize multifunctional particles by using PZS as the "glue" layer to wield the superparamagnetic Fe_3O_4 nanoparticles and Au shells together. The as-prepared particles can simultaneously take advantage of magnetization for MRI imaging diagnosis, as well as strong NIR absorption for photothermal ablation.

2. EXPERIMENTAL SECTION

2.1. Chemicals. Iron(III) acetylacetonate ($Fe(acac)_3$), triethylene glycol (TREG), hexachloro-cyclotriphosphazene (HCCP, 98%), and 4,4′-sulfonyldiphenol (BPS, 98%) were

Received: March 7, 2013
Accepted: May 9, 2013
Published: May 9, 2013

purchased from Aldrich. Triethylamine (TEA), chloroauric acid ($HAuCl_4$), sodium borohydride ($NaBH_4$) and sodium citrate (Na_3Ct) were purchased from Shanghai Chemical Reagent Corporation. Organic solvents, such as tetrahydrofuran (THF), ethyl acetate and anhydrous ethanol, were of analytical grade. All chemicals were used as received without any further purification. Water was purified using a Milli-Q-system (Millipore, Bedford).

2.2. Synthesis of Fe_3O_4@PZS. Water-soluble magnetite nanoparticles were prepared as previously reported.[25] Fe_3O_4 nanoparticles (10 mg), HCCP (40 mg, 115.0 mmol) were added into a 100 mL round-bottom flask. A mixture of THF and anhydrous alcohol (60 mL, 9:1 by volume) and 2.0 mL of TEA were subsequently added. After ultrasonic irradiation for 20 min (50 W, 40 kHz), BPS (90 mg, 360.0 mmol) was then added. The solution was maintained at room temperature for 6 h under ultrasonic irradiation (50 W, 40 kHz). As soon as the reaction was complete, the resulting solids were collected by a magnet, washed with THF and anhydrous alcohol, and dried at 40 °C in a vacuum overnight.

2.3. Synthesis of Fe_3O_4@PZS@Au Seeds. $HAuCl_4$ (1.0 mL, 24.0 mM aqueous solution) was added to an aqueous solution containing 5 mg Fe_3O_4@PZS in an ultrasonic bath (50 W, 40 kHz) at room temperature. After ultrasonication of the mixed solution for 30 min, a 3-fold excess (in molar ratio) of fresh $NaBH_4$ (0.1 wt %) in aqueous sodium citrate (50 mM) was added rapidly with vigorous stirring and the reaction mixture was stirred for an additional 3 min. The resulting Fe_3O_4@PZS@Au seeds were collected with a magnet and washed with distilled water three times. Finally, purified Fe_3O_4@PZS@Au seeds were ultrasonically suspended in water to form a colloidal suspension and the concentration was diluted to 1.0 mg mL^{-1}.

2.4. Seed-Mediated Growth of Au Nanoshells. In the gold shell growth step, Fe_3O_4@PZS@Au seeds (2 mL, 1 mg mL^{-1}) were dissolved in 120 mL of water. After 10 min of stirring, 5 mL of 0.01 M $HAuCl_4$ solution was added. Immediately, the solution was heated to 100 °C with reflux for 10 min, followed by addition of 1.2 mL of 5 wt % Na_3Ct solution with stirring. Over the course of 5 min, the color of the solution changed from light pink to dark blue, which is the nature color of nanoshells.

2.5. Characterization. Transmission electron microscopy (TEM) was carried out on a CM120 (Philips). High resolution-transmission electron microscopy (HR-TEM) was conducted on a JEOL TEM-2100 operating at 200 kV. SAED patterns were collected on HR-TEM. The size and distribution of all as-prepared nanomaterials were determined from TEM micrographs using ImageJ (V1.41, NIH, USA) for image analysis. Photographs were taken with a digital camera (IXUS 800IS, Canon, Japan). Fourier-transform infrared (FTIR) spectra were recorded on a Paragon 1000 (Perkin-Elmer) spectrometer. Samples were dried overnight at 45 °C in vacuum and thoroughly mixed and crushed with KBr to fabricate KBr pellets. XRD patterns were collected on a powder diffractometer (D/max-2200/PC, Rigaku, Japan) using Cu−K radiation. Diffraction patterns were collected from 10° to 90° at a speed of 6°·min^{-1}. The magnetization curves were measured at 300 K under a varying magnetic field with physical property measurement system (PPMS-9T, Quantum Design, USA). The Fe concentration was determined by ICP-AES (VISTAMPXICP Varian, USA). T_2 relaxation time was conducted by PQ001 MRI Analyst (Shanghai Niumag Corporation, China). T_2-weighted images were measured by NMI20-Analyst (Shanghai Niumag Corporation, China). The fluorescence images were recorded using an inverted fluorescence microscope (IX 71, Olympus) and a charge-coupled device (CCD, Cascade 650). Temperature increase experiments were induced using an SDL-808 IR diode collimated laser (SDL, China) with a central wavelength of 808 nm (spot size 5 × 20 mm and output power 1.6 W).

2.6. Measurement of Magnetization Curves, T_2 Relaxation Time and T_2-Weighted Images. Hysteresis cycles at room temperature were performed with a physical property measurement system (PPMS-9T, Quantum Design, USA) from −15 000 to 15 000 Oe. For MRI experiments, samples at given concentrations were suspended in phosphate buffered saline (PBS) and placed in 5 mL tubes. The transverse relaxation time T_2 was measured with varying Fe concentrations using a MRI scanner (PQ001 Analyst, Shanghai Niumag Corporation, China) at a magnetic field strength of 0.5 T. Spin−echo pulse sequences with multiple spin echoes of various echo times were utilized to obtain pixel-by-pixel T_2 maps of each sample (TR/TE, 3000/60 ms; matrix, 15.0 mm × 15.0 mm; section thickness, 0.6 mm). The relaxivities r_2 can be calculated from the slopes of the concentration vs relaxation rate curve. MR imaging capabilities of the Fe_3O_4@PZS and Fe_3O_4@PZS@Au shells were examined at 0.5 T using an NMI20-Analyst (Shanghai Niumag Corporation, China) with the following parameters: TR = 2000 ms, TE = 100 ms, slices =1, slice thickness = 5 mm.

2.7. Biocompatibility of Fe_3O_4@PZS@Au Shell. Human cervical cancer HeLa cells were cultured in Dulbecco's Modified Eagle's medium (DMEM, high glucose) which was supplemented with 10% fetal bovine serum (FBS) in a humidified incubator kept at 37 °C (95% room air, 5% CO_2). Cells were cultured overnight to allow cell attachment and subsequently washed with FBS-free DMEM. Fe_3O_4@PZS, Fe_3O_4@PZS@Au seeds and Fe_3O_4@PZS@Au shell suspensions were then added respectively, and the resulting mixture was incubated at 37 °C for 24 h. The particle concentration in the culture was typically 50 μg mL^{-1}. The cell viability was assessed qualitatively by AO/EB double staining according to the literature.[24]

WST-1 assay was also used to quantitatively assess the biocompatibility of Fe_3O_4@PZS@Au shells. HeLa cells were seeded into a 96-well flat culture plate (Corning). After incubation overnight to allow cell attachment, the cells were incubated with Fe_3O_4@PZS@Au shells (10, 20, 50, 100 μg·mL^{-1}, respectively) in a FBS-free culture medium at 37 °C for 24 and 48 h, respectively. They were subsequently rinsed three times with sterilized PBS. The 200 μL of PBS was used as a substitute for the culture medium before adding 1: 10 (v: v) of the WST-1 reagent. After incubation for another 2 h, the absorbance was measured at 490 nm. Cells cultured without Fe_3O_4@PZS@Au shells at the same time intervals were used as controls.

2.8. TEM Characterization of Fe_3O_4@PZS@Au Shell in Cells. HeLa cells were seeded in a culture dish with a diameter of 60 mm (Corning). The cells were cultured overnight to allow cell attachment, and then incubated with Fe_3O_4@PZS@Au shells (6.3 μg mL^{-1}) in FBS-free culture medium for 12 h. For the TEM analysis, HeLa cells were washed with PBS, and then fixed with 2% glutaraldehyde and 1% osmium tetroxide for 2 h at 48 °C. The cells were then dehydrated in a graded ethanol series (30, 50, 70% with 3% uranyl acetate, 80, 95, and

100%) for 10 min at each concentration followed by two changes in 100% propylene oxide. After infiltration and embedding in epoxy resins at 60 °C for 48 h, the sections were stained with lead citrate and investigated by TEM.

2.9. Photothermal Conversion Experiments. A colloidal aqueous suspension (2.0 mL) stabilized with sodium citrate was placed in a quartz cell ($10 \times 10 \times 40$ mm^3) and exposed to the NIR laser source (1.6 W, spot size 5×20 mm^2) at a distance of 2 cm. The solution temperature was measured using a HT3500C sensitive thermometer.

2.10. Photothermal Hyperthermia on HeLa Cells. Cells were cultured overnight to allow cell attachment. After they were washed with FBS-free DMEM. Fe_3O_4@PZS, Fe_3O_4@PZS@Au seeds and Fe_3O_4@PZS@Au shells suspension was then added and the resulting mixture was incubated at 37 °C for 24 h. The shells concentration in the culture was typically 50 μg mL^{-1}. Before irradiation, the free Fe_3O_4@PZS@Au shells were separated from cultured medium by rinsing three times with PBS. The cells were then treated with a 1.6 W laser diode (spot size: 5×20 mm^2) at a wavelength of 808 nm for 15 min. After irradiation was completed, the cells were rinsed three times with PBS. The cell viability was assessed by AO/EB double staining and WST-1 assay. Stained cells were observed under an inverted fluorescence microscope (IX 71, Olympus) and images were taken using a charge coupled device (CCD, Cascade 650).

3. RESULTS AND DISCUSSION

Scheme 1 illustrates the synthesis procedure. The hydrophilic Fe_3O_4 nanoparticles were prepared according to a modified procedure[25] and dispersed in a mixture of tetrahydrofuran (THF) and ethanol (9: 1, v/v) as a ferrofluid. The Fe_3O_4 nanoparticles were then directly coated with a PZS layer via a facile one-step polymerization of hexachloro-cyclotriphosphazene (HCCP) and 4,4′-sulfonyldiphenol (BPS). When $HAuCl_4$ was reduced by $NaBH_4$ in an aqueous suspension of Fe_3O_4@PZS, the as-prepared gold nanoparticles were ready to attach onto the surface of PZS, because of the metal coordination capability of PZS.[24] And the color of reaction solution changed from gray to purple because of the nature absorption at ca. 520 nm. In the subsequent seed-mediated growth, these gold seeds gradually grew into large ones. And the process was accompanied by adsorption of more gold nanoparticles that formed in the bulk solution. Finally, a dark blue solution was obtained, indicating the formation of the complete gold nanoshells. The as-grown Fe_3O_4@PZS@Au shells can be well-dispersed in water forming a stable suspension for MRI and phototherapy applications.

Scheme 1. Preparation Procedure of Fe_3O_4@PZS@Au Shells

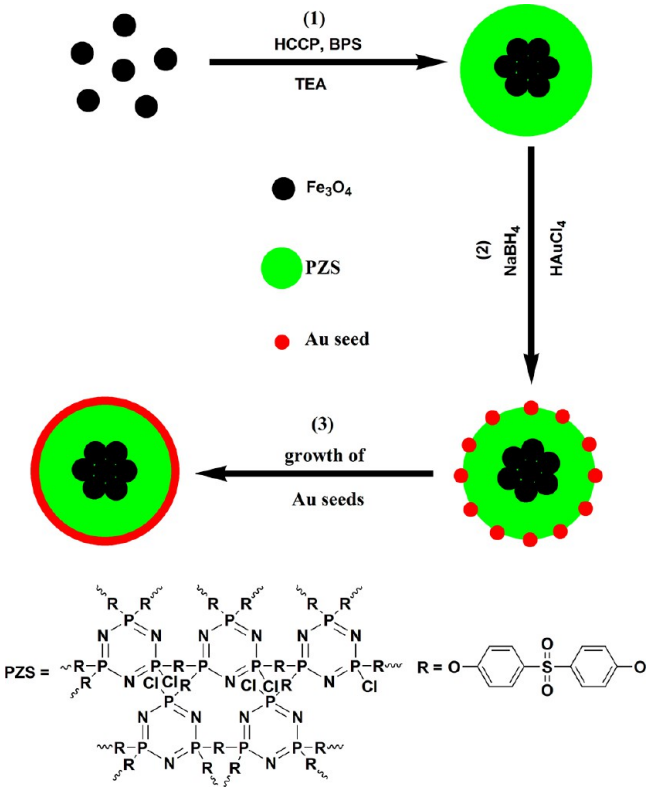

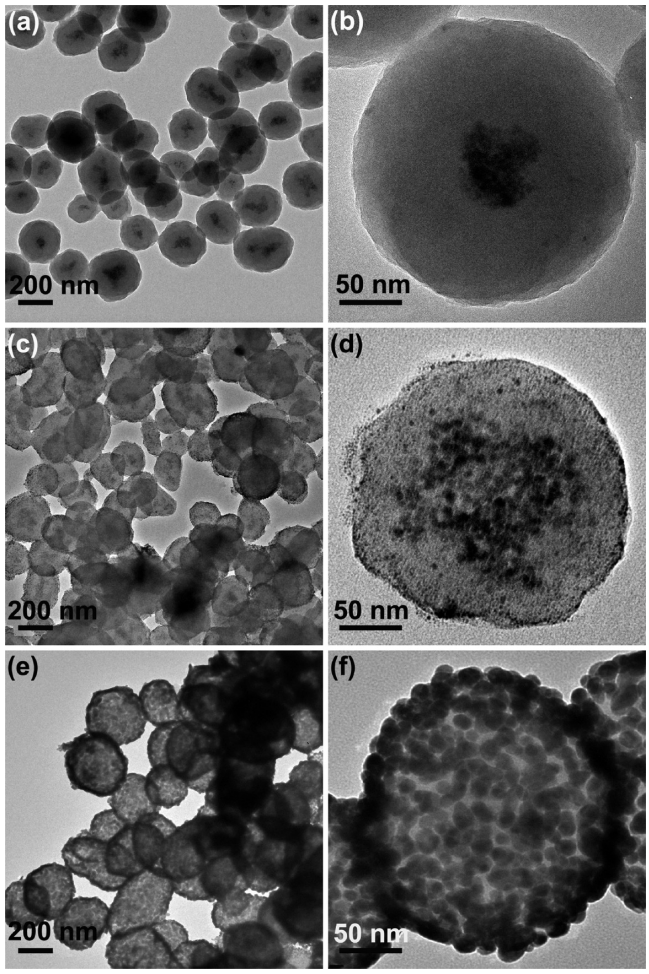

Figure 1. TEM images of (a, b) Fe_3O_4@PZS, (c, d) Fe_3O_4@PZS@Au seeds, and (e, f) Fe_3O_4@PZS@Au shells.

Transmission electron microscopy (TEM) was used to characterize the structure and preparation procedure of Fe_3O_4@PZS@Au shells. The hydrophilic Fe_3O_4 nanoparticles are monodispersed with a diameter of 8.2 ± 1.1 nm (see the Supporting Information, Figure S1a). After the Fe_3O_4 nanoparticles being coated by PZS, the core@shell structure of Fe_3O_4@PZS can be clearly observed because of the different electronic contrast of Fe_3O_4 to PZS (Figure 1a, b). The Fe_3O_4@PZS are about 228.5 ± 15 nm with relatively smooth outer surfaces. And the black cores should be composed of

dx.doi.org/10.1021/am400843d | ACS Appl. Mater. Interfaces 2013, 5, 4586−4591

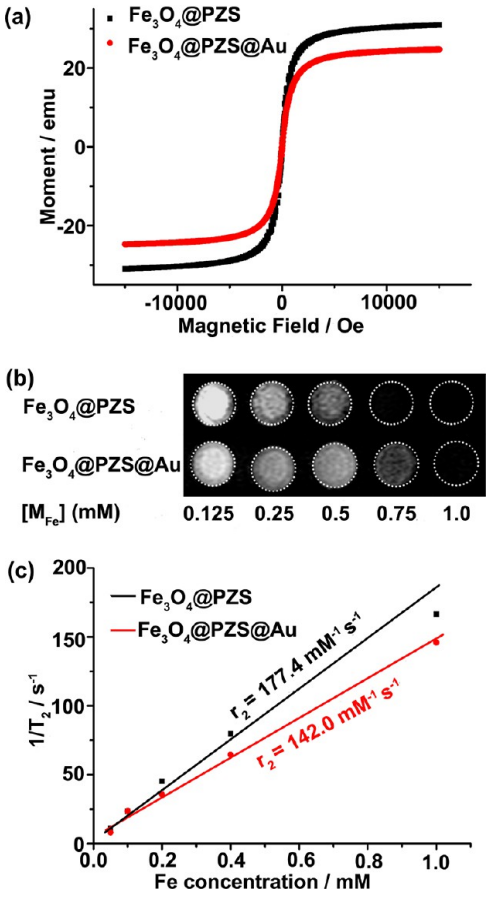

Figure 2. (a) Field-dependent magnetization curve measured at 300 K, (b) T_2-weighted MR images, and (c) T_2 relaxivity plot of aqueous suspension of Fe_3O_4@PZS and Fe_3O_4@PZS@Au shells.

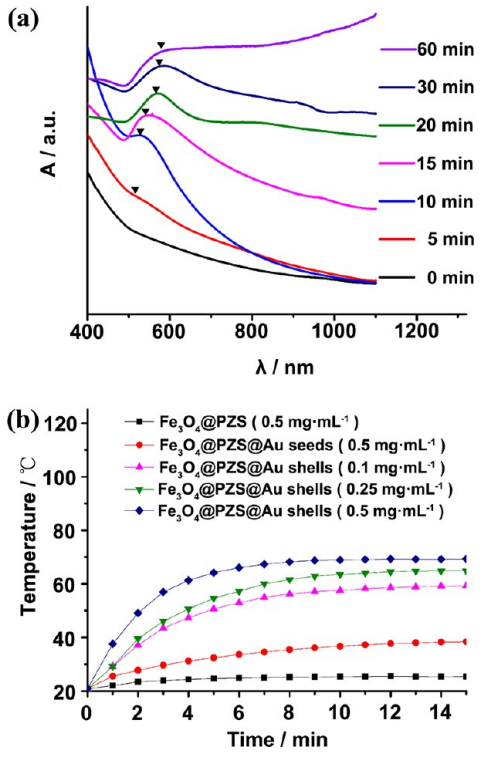

Figure 3. (a) Real-time absorption spectra of Fe_3O_4@PZS@Au shells at different times after addition of $HAuCl_4$ and $NaCt_3$. (b) Photothermal properties of Fe_3O_4@PZS@Au shells under 808 nm laser irradiation at 1.6 W.

many Fe_3O_4 nanoparticles. Interestingly, the size of Fe_3O_4 cores and the thickness of the PZS shell can be easily tuned by varying the mass ratio of Fe_3O_4 to PZS precursors (see the Supporting Information, Figure S1b–d). The gold seeds (~3 nm) were then evenly and firmly attached to the surface of the PZS spheres after rapid reduction of $HAuCl_4$ by $NaBH_4$ (Figure 1c, d). After further reduction of $HAuCl_4$ by Na_3Ct at reflux, continuous Au shells were formed on the Fe_3O_4@PZS by a seed-mediated growth method to give a fine core@shell nanostructure with a diameter of ca. 253 ± 20 nm (Figure 1e, f). The as-grown Fe_3O_4@PZS@Au shells have a relative rough surface that benefits the surface modification and photothermal conversion.

To verify the formation of the Fe_3O_4@PZS@Au shells, Fourier transform infrared (FTIR) spectroscopy, X-ray powder diffraction (XRD), and energy-dispersive X-ray spectroscopy (EDS) were also carried out. The absorption at 943 cm^{-1} for the PZS and Fe_3O_4@PZS is assigned to the P–O–Ar band, indicating the polymerization of comonomers HCCP and BPS.[11] Other characteristic peaks of PZS can also be observed, including 1184 cm^{-1} (P═N), 882 cm^{-1} (P—N) in the cyclotriphosphazene structure; 1284 and 1153 cm^{-1} (O═S═O), 1588 and 1490 cm^{-1} (C═C) in the sulfonylphenol units. However, the intensity of the absorption peaks of PZS greatly decreased for the Fe_3O_4@PZS@Au shells due to the shielding from the outer gold shells (see the Supporting Information, Figure S2a). The Fe_3O_4@PZS possessed one broad diffraction peak and six sharp diffraction peaks, which corresponded to the reflection of PZS and magnetite respectively (see the Supporting Information, Figure S2b). And the XRD patterns of Fe_3O_4@PZS did not show an obvious change after storage in the air for 4 weeks, suggesting that the Fe_3O_4 nanoparticles had a good chemical stability after being coated by PZS. With the gradual increase of Au, gold peaks appeared in the XRD pattern and the peaks for Fe_3O_4 disappeared. The EDS mapping analysis revealed that the component of Fe located in the core was surrounded by the gold shell (see the Supporting Information, Figure S3), suggesting that the Fe_3O_4@PZS@Au core–shell nanostructures were achieved.

The room-temperature magnetization curves of Fe_3O_4@PZS and Fe_3O_4@PZS@Au shells were measured (Figure 2a). The saturation magnetization (Ms) values of the Fe_3O_4@PZS and Fe_3O_4@PZS@Au shells are 30.8 and 24.2 emu g^{-1}, respectively. The Ms decrease of Fe_3O_4@PZS@Au shells could be attributed to the increased mass of the nanoparticle introduced by the gold nanoshell. The two samples are essentially superparamagnetic with negligible hysteresis (see the Supporting Information, Figure S4), suggesting that even though Fe_3O_4 nanoparticles encapsulated in cross-linked PZS and gold shell, they could preserve their superparamagnetic property. The strong magnetization and superparamagnetic property expose these hybrid particles to easy magnetic manipulation (see the Supporting Information, Figure S5). The nanoparticles were rapidly attracted by an external magneticfield, and could be easily redispersed with slight shaking after removal of the magnet. The T_2-weighted MR images of Fe_3O_4@PZS and Fe_3O_4@PZS@Au shell aqueous dispersions at different Fe concentrations were investigated (Figure 2b). While the Fe concentration for the two samples increased, the signal intensity of the MR image decreased. This behavior allows

dx.doi.org/10.1021/am400843d | ACS Appl. Mater. Interfaces 2013, 5, 4586–4591

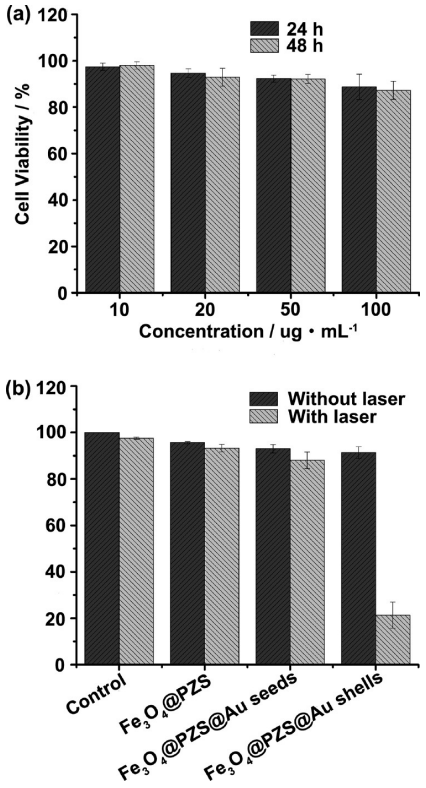

Figure 4. Viability of HeLa cells (a) incubated with Fe_3O_4@PZS and Fe_3O_4@PZS@Au shells at different concentration for 24 and 48 h. (b) with Fe_3O_4@PZS, Fe_3O_4@PZS@Au seeds, and Fe_3O_4@PZS@Au shells at 50 μg mL^{-1} for 24 h with/without 15 min 808 nm laser irradiation (1.6 W). Each values is averaged from seven measurements.

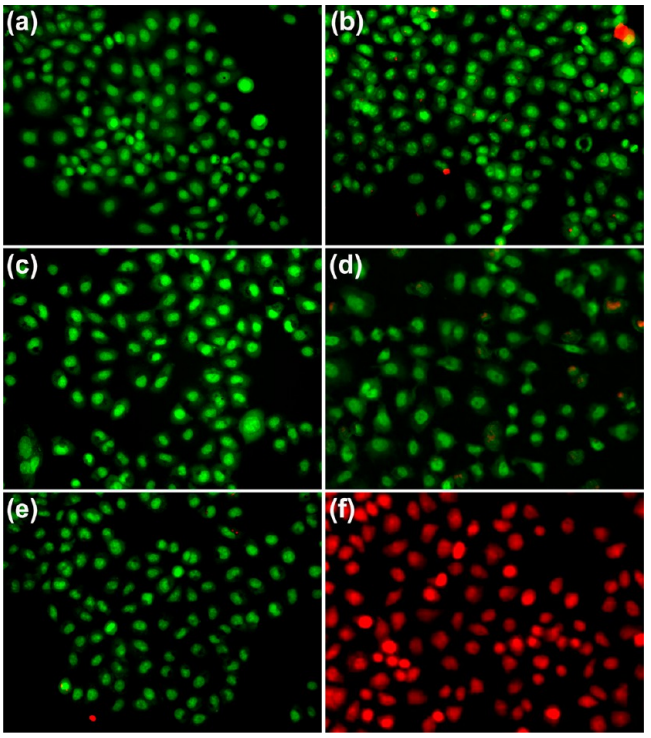

Figure 5. Fluorescence images of HeLa cells (a) control, (b) with 15 min NIR irradiation only, (c) incubated with Fe_3O_4@PZS@Au seeds for 24 h, (d) with both Fe_3O_4@PZS@Au seeds and NIR laser, (e) incubated with Fe_3O_4@PZS@Au shells for 24 h, and (f) with both Fe_3O_4@PZS@Au shells and NIR laser (1.6 W cm^{-2}).

them to be used as T_2 contrast agents, though the T_2-weighted MR images of Fe_3O_4@PZS@Au shell are a little bit brighter than that of Fe_3O_4@PZS at the same Fe concentration. The transverse relaxivity (r_2) of Fe_3O_4@PZS and Fe_3O_4@PZS@Au shell were calculated to be 177.4 and 142 mM^{-1} s^{-1}, respectively (Figure 2c). The r_2 results are comparable with the results reported for the similar nanocomposites,[1,4,11,12] and are well in agreement with that of T_2-weighted MR images.

The UV−vis−NIR absorption spectra of Fe_3O_4@PZS@Au shells at different stages of preparation are shown in Figure 3a. At the initial stage (<5 min), no Plasmon peak was recorded since gold seeds were too small to be a piece of metal with a conduction band but they instead acted as molecules depicted by molecular orbital. With the gradual growth of gold seeds, the maximum absorption peak red-shifted from 526 nm to NIR region accordingly and the color of colloidal suspensions changed from brown to dark blue, which was attributed to the formation of gold shells.

The Fe_3O_4@PZS@Au shells may have important biomedical application for photothermal therapy due to their good water dispersibility and strong NIR SPR absorption. As expected, the aqueous suspensions of Fe_3O_4@PZS@Au shells exhibited a remarkable increase in temperature with exposure time and the temperature approached a plateau at ∼6 min after irradiation by 808 nm laser. The temperature of Fe_3O_4@PZS@Au shell suspension rose rapidly to 66.5 °C within 6 min at the concentration of 0.5 mg·mL^{-1}. Even at low concentration of 0.1 and 0.25 mg mL^{-1}, the temperature also rose to 52.8 and 57.2 °C in 6 min, still high enough to kill cancer cells. In comparison, the aqueous suspensions of Fe_3O_4@PZS and Fe_3O_4@PZS@Au seeds have no obvious elevation of temperature after the NIR laser irradiation. Compared to other works,[19−21] the Fe_3O_4@PZS@Au shells show a more efficient photothermal conversation due to their fine gold nanoshells and the dielectric Fe_3O_4@PZS cores.

The biocompatibility and photothermal therapy of Fe_3O_4@PZS@Au shells were measured by TEM images, WST-1 assay, and AO/EB double staining experiments. The TEM images (see the Supporting Information, Figure S6) show that the Fe_3O_4@PZS@Au shells can be internalized in the Hela cells, localizing mostly in the cytoplasm. Moreover, the HeLa cells exhibit a high tolerance to both Fe_3O_4@PZS and Fe_3O_4@PZS@Au shells after incubation with concentrations of 10−100 μg mL^{-1} for 24 h. The cell viability are all above 90% (Figure 4a), indicating both the samples are biocompatible. The cell viability of HeLa cells treated with 50 μg mL^{-1} Fe_3O_4@PZS or Fe_3O_4@PZS@Au seeds shows negligible change after irradiation by 808 nm laser for 15 min (Figure 4a). However, the cell viability decreases to 21% if the HeLa cells were incubated with Fe_3O_4@PZS@Au shells for 24 h and followed by NIR irradiation for 15 min. We suspected that the Fe_3O_4@PZS@Au shells can effectively absorb NIR laser energy and convert it to heat and the sudden temperature increase triggered the death of the cells. The AO/EB double staining experiments provide another visual proof. Generally, healthy cells have green nuclei and uniform chromatin with an intact cell membrane, whereas the cells in necrosis or at a late stage of apoptosis have red nuclei with a damaged cell membrane.[24] Neither the Fe_3O_4@PZS@Au shells nor the NIR laser irradiation alone can lead to cell death (Figure 5b, e). However, most of the HeLa cells were dead with red nuclei after they were incubated with the Fe_3O_4@PZS@Au shells at the concentration of 50 μg mL^{-1}

dx.doi.org/10.1021/am400843d | ACS Appl. Mater. Interfaces 2013, 5, 4586−4591

for 24 h and followed by 15 min NIR irradiation (Figure 5f). These results are in good agreement with that of WST-1 assay.

4. CONCLUSIONS

In conclusion, we have successfully developed a facile but effective approach for synthesis of core@shell nanostructures with Fe_3O_4 nanoparticles as the inner cores, gold as the shells, and PZS in the mediator. In this structure, the highly cross-linked PZS polymer not only exhibit good water dispersion, biocompatibility and thermal stability, but also provided tailored surface chemistry for the attachment of Au seeds and the following gradual growth of Au shells. The super-paramagnetic Fe_3O_4 cores can provide an efficient contrast agent for MR imaging, while the gold shells act as NIR photothermal therapy converter to kill cancer cells. Therefore, this fine-structured nanocomposite may become an ideal candidate for simultaneous MRI imaging and photothermal therapy and has a great potential for biosensors, catalysts, and other applications.

■ ASSOCIATED CONTENT

Ⓢ Supporting Information

TEM images of Fe_3O_4 and Fe_3O_4@PZS with different mass ratios of Fe_3O_4 to PZS, FTIR spectra, X-ray diffraction patterns, and elemental mapping profiles analysis of Fe_3O_4@PZS@Au shells, magnified magnetization curves, picture of Fe_3O_4@PZS and Fe_3O_4@PZS@Au shells separation from the solution under an external magnetic field, TEM images of Fe_3O_4@PZS@Au shells in HeLa cells. This material is available free of charge via the Internet at http://pubs.acs.org.

■ AUTHOR INFORMATION

Corresponding Author

*Fax: 86-21-54747535. E-mail: menglingjie@sjtu.edu.cn (L.M.); qhlu@sjtu.edu.cn (Q.L.).

Author Contributions

The manuscript was written through contributions of all authors. All authors have given approval to the final version of the manuscript.

Notes

The authors declare no competing financial interest.

■ ACKNOWLEDGMENTS

This work was supported by National Science Foundation for Distinguished Young Scholars (50925310), the National Science Foundation of China (20874059, 21174087), the Shanghai Municipal Natural Science Foundation (11ZR1448200, 114119a0600), and Evonik Degussa Specialty Chemicals (Shanghai) Co., Ltd. We also thank Prof. Sheng Dong and Mr. Da Xi for their help of magnetic measurement.

■ REFERENCES

(1) Barreto, J. A.; O'Malley, W.; Kubeil, M.; Graham, B.; Stephan, H.; Spiccia, L. *Adv. Mater.* **2011**, *23*, H18.
(2) Bae, K. H.; Chung, H. J.; Park, T. G. *Mol. Cells* **2011**, *31*, 295.
(3) Nasongkla, N.; Bey, E.; Ren, J.; Ai, H.; Khemtong, C.; Guthi, J. S.; Chin, S.-F.; Sherry, A. D.; Boothman, D. A.; Gao, J. *Nano Lett.* **2006**, *6*, 2427.
(4) Ganta, S.; Devalapally, H.; Shahiwala, A.; Amiji, M. *J. Controlled Release* **2008**, *126*, 187.
(5) Liong, M.; Lu, J.; Kovochich, M.; Xia, T.; Ruehm, S. G.; Nel, A. E.; Tamanoi, F.; Zink, J. I. *ACS Nano* **2008**, *2*, 889.
(6) Wang, Y. X. J.; Hussain, S. M.; Krestin, G. P. *Eur. Radiol.* **2001**, *11*, 2319.
(7) Laurent, S.; Forge, D.; Port, M.; Roch, A.; Robic, C.; Elst, L. V.; Muller, R. N. *Chem. Rev.* **2008**, *108*, 2064.
(8) Boyer, D.; Tamarat, P.; Maali, A.; Lounis, B.; Orrit, M. *Science* **2002**, *297*, 1160.
(9) Huang, X. H.; El-Sayed, I. H.; Qian, W.; El-Sayed, M. A. *J. Am. Chem. Soc.* **2006**, *128*, 2115.
(10) Gobin, A. M.; Lee, M. H.; Halas, N. J.; James, W. D.; Drezek, R. A.; West, J. L. *Nano Lett.* **2007**, *7*, 1929.
(11) Dickerson, E. B.; Dreaden, E. C.; Huang, X.; El-Sayed, I. H.; Chu, H.; Pushpanketh, S.; McDonald, J. F.; El-Sayed, M. A. *Cancer Lett.* **2008**, *269*, 57.
(12) Choi, W. I.; Kim, J.-Y.; Kang, C.; Byeon, C. C.; Kim, Y. H.; Tee, G. *ACS Nano* **2011**, *5*, 1995.
(13) Day, E. S.; Thompson, P. A.; Zhang, L.; Lewinski, N. A.; Ahmed, N.; Drezek, R. A.; Blaney, S. M.; West, J. L. *J. Neurooncol.* **2011**, *104*, 55.
(14) Lal, S.; Clare, S. E.; Halas, N. J. *Acc. Chem. Res.* **2008**, *41*, 1842.
(15) Chen, J.; Wang, D.; Xi, J.; Au, L.; Siekkinen, A.; Warsen, A.; Li, Z.-Y.; Zhang, H.; Xia, Y.; Li, X. *Nano Lett.* **2007**, *7*, 1318.
(16) Chen, J.; Glaus, C.; Laforest, R.; Zhang, Q.; Yang, M.; Gidding, M.; Welch, M. J.; Xia, Y. *Small* **2010**, *6*, 811.
(17) Xia, Y.; Li, W.; Cobley, C. M.; Chen, J.; Xia, X.; Zhang, Q.; Yang, M.; Cho, E. C.; Brown, P. K. *Acc. Chem. Res.* **2011**, *44*, 914.
(18) Chen, J.; Guo, Z.; Wang, H.-B.; Gong, M.; Kong, X.-K.; Xia, P.; Chen, Q.-W. *Biomaterials* **2013**, *34*, 571.
(19) Kim, J.; Park, S.; Lee, J. E.; Jin, S. M.; Lee, J. H.; Lee, I. S.; Yang, I.; Kim, J.-S.; Kim, S. K.; Cho, M.-H.; Hyeon, T. *Angew. Chem., Int. Ed.* **2006**, *45*, 7754.
(20) Yang, Y.; Mahdavian, A. R.; Daniels, E. S.; Klein, A.; El-Aasser, M. S. *J. Appl. Polym. Sci.* **2013**, *127*, 3768.
(21) Dong, W.; Li, Y.; Niu, D.; Ma, Z.; Gu, J.; Chen, Y.; Zhao, W.; Liu, X.; Liu, C.; Shi, J. *Adv. Mater.* **2011**, *23*, 5392.
(22) Fu, J.; Huang, X.; Huang, Y.; Pan, Y.; Zhu, Y.; Tang, X. *J. Phys. Chem. C* **2008**, *112*, 16840.
(23) Zhou, J.; Meng, L.; Lu, Q.; Fu, J.; Huang, X. *Chem. Commun.* **2009**, 6370.
(24) Zhou, J.; Meng, L.; Lu, Q. *J. Mater. Chem.* **2010**, *20*, 5493.
(25) Wan, J.; Cai, W.; Meng, X.; Liu, E. *Chem. Commun.* **2007**, 5004.